ChemPubSoc Europe

DOI: 10.1002/ejic.201901083

EurJIC European Journal of Inorganic Chemistry

Full Paper

Ion Conducting Phosphidosilicates

Synthesis and Structure of the Sodium Phosphidosilicate Na_2SiP_2

Arthur Haffner,[a] Anna-Katharina Hatz,[a,b] Constantin Hoch,[a] Bettina V. Lotsch,[a,b] and Dirk Johrendt*[a]

Abstract: Ion conductors of light alkaline metals based on earth-abundant elements are important components for all-solid-state batteries. The new sodium-rich phosphidosilicate Na_2SiP_2 was synthesized by solid state reaction of stoichiometric amounts of the elements at 973 K and characterized by single-crystal X-ray diffraction (space group *Pccn* (no. 56), a = 12.7929(5) Å, b = 22.3109(9) Å, c = 6.0522(2) Å and Z = 16) and solid-state NMR under MAS conditions. The compound forms dark-red twinned crystals, and its crystal structure contains edge-sharing SiP_4 tetrahedra connected to infinite $_\infty^1[SiP_{4/2}]$ chains. The sodium ions between the chains are fairly mobile. Electrochemical impedance spectroscopy shows a total ionic conductivity of $\sigma(Na^+, 373\ K) = 2.3\ ?\ 10^{-6}\ Scm^{-1}$ with an activation energy of E_a = 0.43 eV, and the galvanostatic polarization reveals mixed conduction behavior with a transference number of 0.8.

Introduction

Fast lithium and sodium ion conductors composed of earth abundant elements as potential components of all solid-state batteries attract immense interest.[1–5] Recently, several phosphidosilicates with isolated or condensed SiP_4 tetrahedra have demonstrated lithium or sodium ion conductivity, for example Li_8SiP_4,[6] Li_2SiP_2,[6,7] $LiSi_2P_3$,[7] and the series $Na_{23}Si_{9n+19}P_{12n+33}$ (n = 0–3).[8] These compounds have also been studied in the framework of the electrochemical mechanism of SiP_2/Li anodes.[9,10] Except Li_8SiP_4 with isolated $[SiP_4]^{8-}$ tetrahedra, the crystal structures feature networks of interpenetrating T2–T5 supertetrahedra according to the *Yaghi* notation.[7,8,11] It was shown that larger supertetrahedral entities favor the ion conductivity by diluting the alkali metal ions between the lower charged clusters.[8] Nevertheless there is currently no reason to believe that supertetrahedral structures are generally needed for facile ion movement in phosphidosilicates. Since the actual structural requirements for fast ion conductivity are still not fully understood, it is reasonable to search for further compounds in this system. The supertetrahedral compounds in the system Na-Si-P are rather sodium-poor and the only known sodium-rich compound is Na_5SiP_3.[12] Therefore we focused on the sodium-rich part of the system and came across Na_2SiP_2 which turned out to be structurally quite different from the lithium analogue reported earlier.[6,7] Here we report the synthesis, crystal structure, NMR and impedance spectroscopy of Na_2SiP_2.

Results and Discussion

The crystal structure of Na_2SiP_2 was solved from single-crystal diffraction data using direct methods.[13] The diffraction patterns of several measured single-crystals showed pseudo-hexagonal metric, but a structure solution using hexagonal symmetry failed. One specimen showed unequal contributions of the twin domains, so the feigned hexagonal intensity distribution was broken. From this dataset, a structure model with orthorhombic symmetry could be derived under the assumption of a merohedral *drilling* by a rotation of 120° around (0 0 1). From the expected three sets of *drilling* domains, only two were observed in the diffraction pattern. One additional domain occurs twinned by the mirror plane (1 1 0) yielding in volume fractions of 16.8 and 13.5 %. Note that this twinning originates not from phase transitions but is caused by the metric of the orthorhombic unit cell ($b/a \approx \sqrt{3}$), leading to oriented adhering of crystal domains while growth of the contact twins. Figure 1 (left) shows the pseudo-hexagonal diffraction pattern of the *hk*2 plane with the three interfering lattices marked in blue (main domain), green and purple (minor components). The reflections of the main domain show little intensity deviations (a, highlighted in red) compared to the other two highlighted areas (b and c), where only every second reflection belongs to the main component, discernible by alternating intensities. Figure 1 (right) shows a non-integer 0.5*kl*-plane, where no reflections of the main domain are visible, but of the two minor components.

[a] *Department of Chemistry, Ludwig-Maximilians-University of Munich, Butenandtstr. 5-13 (D), 81377 Munich, Germany*
E-mail: johrendt@lmu.de
[b] *Department of Nanochemistry, Max Planck Institute for Solid State Research,*
Heisenbergstr. 1, 70569 Stuttgart, Germany
ORCID(s) from the author(s) for this article is/are available on the WWW under https://doi.org/10.1002/ejic.201901083.

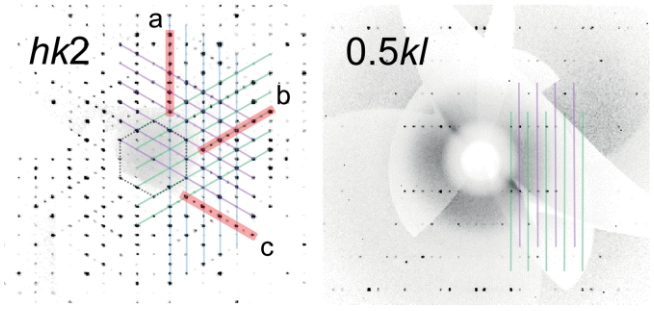

Figure 1. Left: *hk*2-plane with the three interfering lattices marked blue (main component), green and purple (minor components). The red highlighted areas indicate the violation of the hexagonal symmetry. Right: 0.5*kl*-plane with reflections of the two minor components only.

All atom positions were refined with anisotropic thermal displacement parameters. Data on structure refinement and the fractional coordinates are compiled in Table 1 and Table 2 (CCDC 1946908).

Table 1. Crystallographic data for the refinement of Na_2SiP_2.

Formula	Na_2SiP_2
formula mass/g mol^{-1}	136.01
space group	*Pccn* (no. 56)
a/Å	12.7929(5)
b/Å	22.3109(9)
c/Å	6.0522(2)
V/Å^3	1727.43(11)
Z	16
$\rho_{X\text{-ray}}$/g cm^{-1}	2.092
μ/mm^{-1}	1.262
radiation	Mo-K_α
θ-range/°	3.168–30.682
reflections measured	28523
independent reflections	4104
refined parameters	94
R_σ	0.0225
R_{int} (main component)	0.0404
*R*1 ($F^2 > 2\sigma(F^2)$/all)	0.0389/0.0455
w*R*2 ($F^2 > 2\sigma(F^2)$/all)	0.0852/0.0881
GooF	1.118
BASF factor 1	0.16745
BASF factor 2	0.13472
$\Delta\rho_{max}$, $\Delta\rho_{min}$/e Å^3	0.634, –1.460

Table 2. Fractional atom coordinates, Wyckoff positions and equivalent displacement parameters of Na_2SiP_2.

Atom	Wyckoff position	*x*	*y*	*z*	U_{eq}/Å^2
P1	8*e*	0.03221(7)	0.07405(4)	0.00206(16)	0.01376(16)
P2	8*e*	0.12998(6)	0.50881(4)	0.00362(16)	0.01327(15)
P3	8*e*	0.16116(7)	0.19518(4)	0.43788(14)	0.01279(16)
P4	8*e*	0.66053(8)	0.19606(5)	0.18775(16)	0.0198(2)
Si1	8*e*	0.50140(8)	0.00021(5)	0.25362(14)	0.01086(15)
Si2	4*d*	1/4	3/4	0.0615(3)	0.0157(3)
Si3	4*c*	1/4	1/4	0.1882(2)	0.0102(2)
Na1	8*e*	0.00974(14)	0.20996(8)	0.0224(3)	0.0330(4)
Na2	8*e*	0.24880(16)	0.08638(8)	0.2294(3)	0.0275(3)
Na3	8*e*	0.30558(15)	0.59216(9)	0.0123(4)	0.0408(5)
Na4	8*e*	0.50940(12)	0.11973(7)	0.0096(3)	0.0272(3)

The phosphidosilicate polyanion in Na_2SiP_2 is composed of three crystallographically independent SiP_4 tetrahedra, sharing common edges along [001] and assembling three independent $_\infty^1[SiP_2]^{2-}$ chains (Figure 2). The Si–P distances range between 2.244 and 2.273 Å as typical in phosphidosilicates. With 94.98 to 121.95°, the P–Si–P angles show considerable deviation from the ideal tetrahedral angle, whereas the mean value of 109.77° is still close to it. The sodium cations reside on general Wyckoff positions between the tetrahedra chains coordinated by P atoms and form distorted trigonal bipyramids (Na1), octahedra (Na2 and Na4) or trigonal prisms (Na3) with two elongated Na–P distances (see Figure 3). The measured reflection patterns indicated a hexagonal crystal symmetry in which no structure solution was possible. The underlying hexagonal motif appears in the topology of a hexagonal rod packing of the anionic bars along the *c*-axis (Figure 4) as well as in the *b*/*a* ratio with only 0.69 % deviation from √3. By decorating these bars with silicon and phosphorus ions to edge-shared $_\infty^1[SiP_2]^{2-}$ chains, the hexagonal symmetry reduces to orthorhombic with splitting into three crystallographically independent SiP_2 chains. The symmetry reduction creates a pseudo-merohedral *drilling* with a *C*-centered orthorhombic unit cell. For the tetrahedra chain composed of Si1, P1 and P2 this centering is nearly accomplished whereas it is infringed by the two other tetrahedra chains. As depicted in Figure 4, the tetrahedra chain with Si3 slightly shift along [001] whereas the symmetry equivalent chain displaces in the opposing direction. The same occurs in the chain assem-

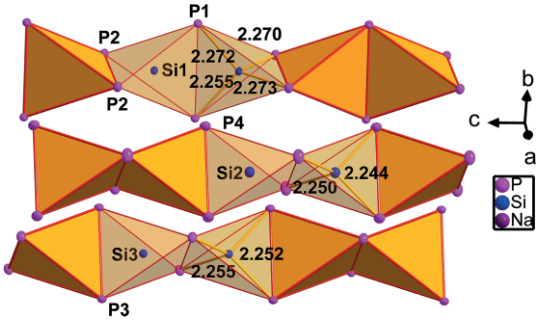

Figure 2. Three independent $_\infty^1[SiP_2]^{2-}$ chains of edge-sharing SiP_4 tetrahedra in Na_2SiP_2 with Si–P distances.

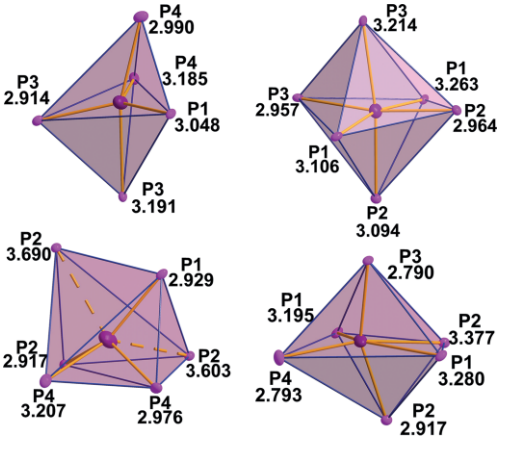

Figure 3. Distorted NaP_x polyhedra in Na_2SiP_2 (top, left: $Na1P_5$ trigonal bipyramid; top, right: $Na2P_6$ octahedron; bottom, left: $Na3P_6$ trigonal prism; bottom, right: $Na4P_6$ octahedron).

bled of Si2 and P4 with a larger offset. In case of the sodium ions the discussed centering is also valid if a minor displacement is taken into account.

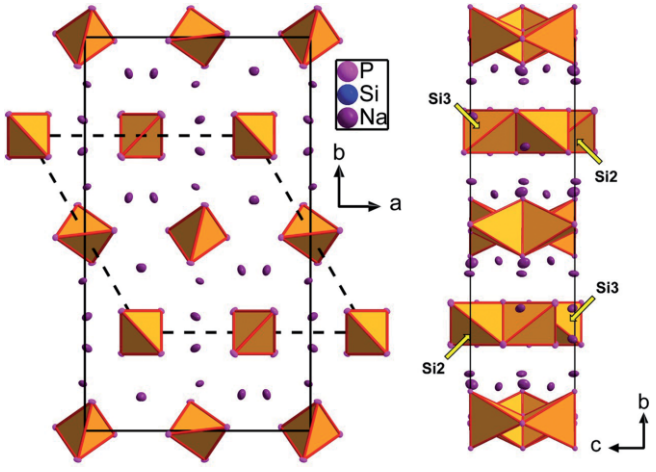

Figure 4. Unit cell of Na_2SiP_2 with $_\infty^1[SiP_2]^{2-}$ tetrahedra chains in [001] direction and the pseudo-hexagonal unit cell (left) and view along the *a*-axis with opposing displacement of the tetrahedral chains (right).

In contrast to Li_2SiP_2,[7] where the constituting SiP_4 tetrahedra assemble interpenetrating T2 supertetrahedral networks, the structural motifs of K_2SiP_2[14] and Cs_2SiP_2[15] with K_2ZnO_2-type structure[16] are rather similar to Na_2SiP_2, where the tetrahedra chains are arranged along the *c*-axis as well. Due to the chain orientation with respect to the *ab*-plane there are two differently oriented, but topologically identical chains in K_2SiP_2 whereas in Na_2SiP_2 three types occur (symmetrically inequivalent due to shift in the *z* parameter, Figure 4) leading to nearly the same *c*- and almost doubled *a* and *b* cell parameters involving quadruplicating of respective Wyckoff sites. The majority of representatives of the K_2ZnO_2-type structure are sulfides or selenides with relatively big cations separating the tetrahedra chains like in A_2CoX_2[17] or A_2MnX_2[18] or in the compounds $A_3Fe_2X_4$[19–21] (*A* = K, Rb, Cs; *X* = S, Se) with the $Tl_3Fe_2S_4$-type structure. There are fewer examples of tetrahedra chains surrounded by cations smaller than potassium like in Na_2ZnS_2,[22] $Na_2Co(S;Se)_2$[17] or $Na_3Fe_2(S;Se)_4$.[23,24] Decreasing the amount of the separating counterions leads to $KFeSe_2$-type structure[25] with edge condensed tetrahedra chains as well. The effect of substitution of Cs^+ in $CsGa(S;Se)_2$ by smaller cations Rb^+ or K^+ was investigated, and it turned out that the structure changes when about 30 % of the Cs^+ ions are replaced.[26] These findings may suggest that chains of edge condensed tetrahedra are stabilized by the amount and size of the counterions.

NMR spectra of all constituting nuclei were collected under MAS conditions with rotation frequencies of 10 kHz of a pure polycrystalline sample (see Figure 5). As depicted in Figure 6, Na_2SiP_2 has four resonance frequencies for phosphorus at δ (^{31}P) = –74.7, –71.4, –52.6 and –34.8 ppm with the first two at nearly the same chemical shift. Integrating the intensities including rotation sidebands yields a 1:1:1:1 ratio indicating four magnetically inequivalent phosphorus atoms in the structure. The resonances with nearly the same chemical shift are assigned to P3 and P4 with almost the same Si–P distances and both with five sodium ions in vicinity. P3 induces the resonance in the shielded region due to the larger chemical shift anisotropy than P4, seen on the greater intensity on the rotation sideband pattern, whereas the downfield signals belong to the Si1 tetrahedra chain with slightly elongated Si–P distances. Following the observation described by Monconduit et al. for compounds in the Li-Si-P system, a resonance is shifted into the upfield region with increasing negative charge density at a particular phosphorus atom in ^{31}P-NMR spectra.[9] Assuming the same behavior towards sodium ions, the resonance at δ (^{31}P) = –52.6 ppm can be assigned to P2 with seven by contrast to P1 with six sodium ions in vicinity (the limit was set to 3.7 Å for this approach). In the silicon spectrum three broad resonances were detected in agreement with the structure model at δ (^{29}Si) = –59.0, –39.3 and –35.5 ppm. The additional signal at 48 ppm differs in line shape and is assigned to background noise. Opposing the structure model, in the sodium spectrum only one signal is visible with a shoulder in the high field region

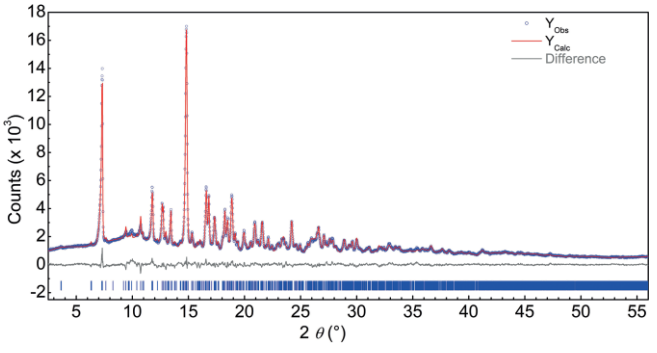

Figure 5. X-ray powder pattern of Na_2SiP_2 (blue) with Rietveld fit (red) and difference plot (grey).

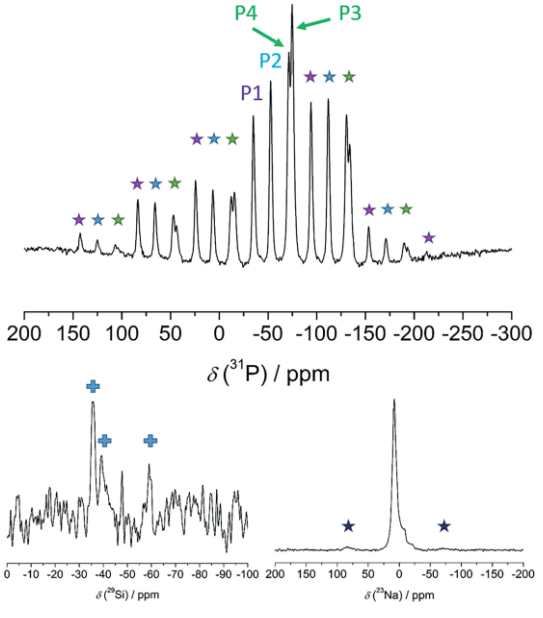

Figure 6. ^{31}P (top), ^{29}Si (bottom, left) and ^{23}Na (bottom, right) MAS-NMR spectra at 10 kHz of Na_2SiP_2 with star-marked rotation side bands. Respective chemical shifts are δ (^{31}P) = –74.7, –71.4, –52.6 and –34.8 ppm, δ (^{29}Si) = –59.0, –39.3 and –35.5 ppm (marked with crosses) and δ (^{23}Na) = 8.1 ppm.

at δ (^{23}Na) = 8.1 ppm instead of four distinct resonances. As it was shown for sodium based supertetrahedral ionic conductors,[8] this observation can arise from similar chemical environment or from fast exchange processes. Since Na_2SiP_2 comprises three different NaP_x polyhedra, one single sodium resonance indicates fast dynamics.

Ionic conduction was quantified by electrochemical impedance spectroscopy. Spectra measured from 303 to 373 K (cf. Figure 7a) reveal two distorted semicircles at higher frequencies and a spike at lower frequencies which results from polarization of sodium ions at the blocking electrodes. The data were fitted to the equivalent circuit shown in Figure 7b comprising of two parallel resistances (R) and constant phase element (CPE)- entities, representing the semicircles, in series to a CPE for the electrode polarization. These elements are placed in parallel to a capacitor (C) representing a stray capacitance of about 80 pF. According to the Brug formula $C_{eff} = Q^{1/\alpha} R^{(1/\alpha-1)}$ an effective capacitance (C_{eff}) of a CPE in parallel to a resistance was calculated resulting C_{eff}(CPE1) = 30 pF and C_{eff}(CPE2) = 0.23 nF.[27] These values indicate that only grain boundary processes or current constriction phenomena are visible.[28,29] The bulk properties could not be resolved and only the total ionic conductivity σ (Na^+) of 2.3×10^{-6} Scm^{-1} at 373 K was calculated from the sum of R1 + R2 = R by σ (Na^+) = $L\cdot(RA)^{-1}$ with L being the thickness and A the area of the sample. Since the grain boundary thickness is unknown, the activation energies of the two processes were calculated with the conductivity derived from the formula above using R1 and R2, respectively. A low activation energy of 0.43 eV for the high frequency process (CPE1R1) and a significantly higher one of 0.57 eV for CPE2R2, possibly stemming from highly resistive grain boundaries, were obtained. The DC galvanostatic polarization measurement in Figure 7d, measured with stainless steel electrodes at 368 K, determines an electronic conductivity of σ (e^-) = 7.9×10^{-9} Scm^{-1}, which is roughly one order of magnitude lower than the σ (Na^+) of 6.8×10^{-8} Scm^{-1} of this sample leading to a transference number of 0.8. This classifies the material as a sort of mixed ionic electronic conductor being unsuitable for the application as solid electrolyte, but potentially interesting in SiP_2 electrode material research.

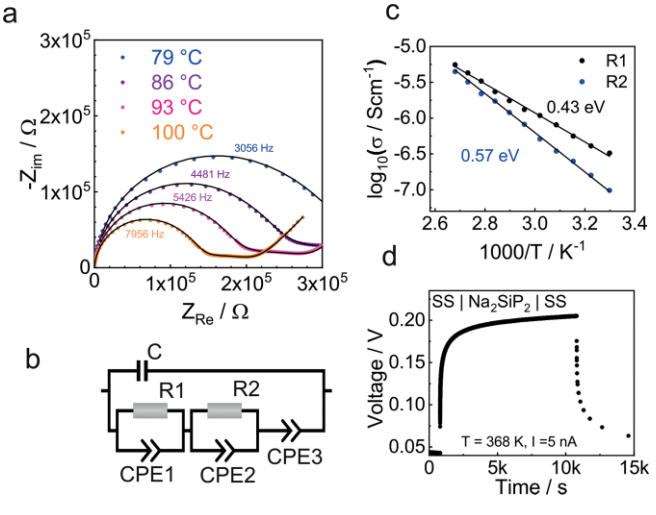

Figure 7. (a) Selection of temperature dependent AC impedance spectra of Na_2SiP_2 fitted to the equivalent circuit shown in (b). (c) Plot of the activation energy showing 0.43 eV for R1 in parallel CPE ≈ 3×10^{-11} F and 0.57 eV for R2 in parallel to CPE ≈ 2×10^{-10} F (d) DC galvanostatic polarization measured with stainless steel electrodes showing a σe^- of 7.9×10^{-9} S/cm at 368 K.

Conclusions

Na_2SiP_2 is a new phosphidosilicate with a SiS_2-like arrangement of $_\infty^1[SiP_2]^{2-}$ chains and fairly mobile sodium ions between them. The crystal structure differs from the related potassium compound with K_2ZnO_2-type structure by three crystallographically different tetrahedra chains instead of one and feigns hexagonal symmetry. Impedance data show mobile sodium ions at elevated temperatures and polarization experiments reveal mixed ionic and electronic conduction behavior, making this compound potentially interesting in SiP_2 electrode material research. Na_2SiP_2 enriches the family of phosphidosilicates and encourages continuing research in the field of the Si-P-system with light alkali metals for low-cost energy storage applications.

Experimental Section

Synthesis. Na_2SiP_2 was prepared by solid-state reaction of a stoichiometric mixture of metallic sodium (67.6 mg, Alfa Aesar, 99.8 %), silicon powder (41.3 mg, Smart Elements, 99.8 %) and red phosphorus (91.1 mg, Chempur, > 99 %). The reaction mixture was ground and filled in alumina crucibles under inert conditions in an argon-filled glovebox with concentrations of O_2 and H_2O < 0.1 ppm. This mixture was sealed in a silica ampoule and fired in a tube furnace to 100 °C within 5 h before the temperature was raised to 700 °C and maintained for 40 h. After cooling to room temperature, the still inhomogeneous product was ground thoroughly and reheated to the same reaction temperature twice yielding a polycrystalline and highly moisture-sensitive red powder.

Single-Crystal X-ray Diffraction

Crystals of sufficient quality for diffraction experiments were selected under dried paraffin oil and sealed in oil-filled glass capillaries (Hilgenberg GmbH, Malsfeld, Germany, inner diameter 0.1 mm). Diffraction data were collected on a Bruker D8 Quest diffractometer equipped with a microfocus Mo-K_α X-ray source, Göbel mirror optics and Photon II detector. For data reduction and absorption correction the software package APEX3[30] was used. Space group determination was carried out with XPREP[31] based on systematically absent reflections. SHELX-97[13] was used for structure solution and refinement. Visualization of the crystal structure was carried out with Diamond[32] software.

CCDC 1946908 (for Na_2SiP_2) contains the supplementary crystallographic data for this paper. These data can be obtained free of charge from The Cambridge Crystallographic Data Centre.

Powder X-ray Diffraction. For powder X-ray diffraction a phase pure polycrystalline sample was ground and sealed in Hilgenberg glass capillaries to avoid hydrolysis. Data were collected on a Stadi P powder diffractometer (STOE & Cie GmbH, Darmstadt, Germany) equipped with a Mythen 1K detector (Dectris, Baden, Switzerland) in Debye-Scherrer geometry with a Ge(111) monochromator and Mo-$K_{\alpha1}$ radiation. Rietveld refinement based on single-crystal diffraction data was performed with TOPAS[33] software.

Solid-State MAS-NMR. Polycrystalline samples of Na_2SiP_2 were loaded into a commercial 4 mm zirconia rotor. Spectra of ^{23}Na, ^{29}Si and ^{31}P were acquired on a Bruker Avance III 500 with a magnetic field of 11.74 T in MAS conditions (ν_{rot} = 10 kHz) and Larmor frequencies of $\nu_0(^{23}Na)$ = 132.33 MHz, $\nu_0(^{29}Si)$ = 99.38 MHz and $\nu_0(^{31}P)$ = 202.48 MHz. All spectra were indirectly referenced to ^1H in 100 % TMS at –0.1240 ppm.

Electrical Conductivity. For DC conductivity measurements and AC impedance spectroscopy, an Ivium compactstat.h (24 bit) in a two-electrode setup using a home-build Swagelok cell was applied. Prior to the measurements a polycrystalline sample was compacted to a pellet with 5 mm in diameter and 1 mm of thickness by uniaxial cold pressing (22 kN) and annealed for 10 h at 400 °C. Then, the pellet was sandwiched between indium foil (Alfa Aesar, 0.127 mm of thickness, 99.99 %) to enhance contact with the Swagelok cell. No reactions between the pellet and the indium foil were observed. For DC measurements stainless steel electrodes were applied. All measurements were carried out under inert conditions and the amplitude of the AC voltage was 100 mV. Collected data were analyzed by RelaxIS3 software from rhd instruments.

Acknowledgments

The authors thank Christian Minke and Otto Zeman for assistance and advices with MAS-NMR measurements. Financial support by the University of Munich (LMU), the Max Plank Society, the Center for NanoScience (CeNS), the Cluster of Excellence e-conversion, and not least the Deutsche Forschungsgemeinschaft (DFG) are gratefully acknowledged. Further financial support was granted by the German Federal Ministry of Research and Education (BMBF), project 03XP0177B (FestBatt).

Keywords: Sodium · Phosphidosilicates · Ion conductivity · Solid-state electrolytes · Structure elucidation

[1] F. Zheng, M. Kotobuki, S. Song, M. O. Lai, L. Lu, *J. Power Sources* **2018**, *389*, 198–213.
[2] R. Chen, W. Qu, X. Guo, L. Li, F. Wu, *Mater. Horiz.* **2016**, *3*, 487–516.
[3] Y. Wang, S. Song, C. Xu, N. Hu, J. Molenda, L. Lu, *Nano Mater. Sci.* **2019**, *1*, 91–100.
[4] B. V. Lotsch, J. Maier, *J. Electroceram.* **2017**, *38*, 128–141.
[5] Z. Zhang, Y. Shao, B. V. Lotsch, Y.-S. Hu, H. Li, J. Janek, L. F. Nazar, C.-W. Nan, J. Maier, M. Armand, L. Chen, *Energy Environ. Sci.* **2018**, *11*, 1945–1976.
[6] L. Toffoletti, H. Kirchhain, J. Landesfeind, W. Klein, L. van Wüllen, H. A. Gasteiger, T. F. Fässler, *Chem. Eur. J.* **2016**, *22*, 17635–17645.
[7] A. Haffner, T. Bräuniger, D. Johrendt, *Angew. Chem. Int. Ed.* **2016**, *55*, 13585–13588; *Angew. Chem.* **2016**, *128*, 13783.
[8] A. Haffner, A.-K. Hatz, I. Moudrakovski, B. V. Lotsch, D. Johrendt, *Angew. Chem. Int. Ed.* **2018**, *57*, 6155–6160; *Angew. Chem.* **2018**, *130*, 6263.
[9] G. Coquil, B. Fraisse, N. Dupré, L. Monconduit, *ACS Appl. Energy Mater.* **2018**, *1*, 3778–3789.
[10] D. Duveau, S. S. Israel, J. Fullenwarth, F. Cunin, L. Monconduit, *J. Mater. Chem. A* **2016**, *4*, 3228–3232.
[11] H. Li, J. Kim, T. L. Groy, M. O'Keeffe, O. M. Yaghi, *J. Am. Chem. Soc.* **2001**, *123*, 4867–4868.
[12] B. Eisenmann, M. Somer, *Z. Naturforsch. B* **1985**, *40*, 886–890.
[13] G. M. Sheldrick, *Acta Crystallogr., Sect. A* **2008**, *64*, 112–122.
[14] B. Eisenmann, M. Somer, *Z. Naturforsch. B* **1984**, *39*, 736–738.
[15] B. Eisenmann, J. Klein, *J. Less-Common Met.* **1991**, *175*, 109–117.
[16] E. Vielhaber, R. Hoppe, *Z. Anorg. Allg. Chem.* **1968**, *360*, 7–14.
[17] W. Bronger, C. Bomba, *J. Less-Common Met.* **1990**, *158*, 169–176.
[18] W. Bronger, H. Balk-Hardtdegen, D. Schmitz, *Z. Anorg. Allg. Chem.* **1989**, *574*, 99–106.
[19] W. Bronger, U. Ruschewitz, P. Müller, *J. Alloys Compd.* **1995**, *218*, 22–27.
[20] W. Bronger, H. S. Genin, P. Müller, *Z. Anorg. Allg. Chem.* **1999**, *625*, 274–278.
[21] K. O. Klepp, S. Pantschov, H. Boller, *Z. Kristallogr.* **2000**, *215*, 5–6.
[22] K. O. Klepp, W. Bronger, *Rev. Chim. Miner.* **1983**, *20*, 682–688.
[23] H. Boller, H. Blaha, *Monatsh. Chem.* **1983**, *114*, 145–154.
[24] K. O. Klepp, W. Sparlinek, *Z. Kristallogr.* **1996**, *211*, 626.
[25] W. Bronger, A. Kyas, P. Müller, *J. Solid State Chem.* **1987**, *70*, 262–270.
[26] D. Friedrich, M. Schlosser, M. Etter, A. Pfitzner, *Crystals* **2017**, *7*, 379.
[27] G. J. Brug, A. L. G. van den Eeden, M. Sluyters-Rehbach, J. H. Sluyters, *J. Electroanal. Chem.* **1984**, *176*, 275–295.
[28] J. T. S. Irvine, D. C. Sinclair, A. R. West, *Adv. Mater.* **1990**, *2*, 132–138.
[29] J. Fleig, J. Maier, *J. Am. Ceram. Soc.* **1999**, *82*, 3485–3493.
[30] *APEX3*, Version 2016.5–0, Bruker AXS Inc., Madison, Wisconsin, **2016**.
[31] *XPREP*, Version 2008/2, Bruker AXS Inc., Karlsruhe, Germany, **2008**.
[32] K. Brandenburg, *Diamond*, Version 3.2k, Crystal Impact GbR, Bonn, Germany, **2014**.
[33] A. Coelho, *TOPAS-Academic*, Version 4.1, Coelho Software, Brisbane, Australia, **2007**.

Received: October 8, 2019